5-1-2013

Manufacturing Gallium Doped ZnO Thin Films Suitable for Use in Thin Film Transistors Using Unbalanced Magnetron Sputtering

Timothy Russell Jones
Southern Illinois University Carbondale, tjones@siu.edu

MANUFACTURING GALLIUM DOPED ZnO THIN FILMS SUITABLE FOR USE IN THIN FILM TRANSISTORS USING UNBALANCED MAGNETRON SPUTTERING

by

Timothy R Jones

BA, St John's College at Annapolis, 2008

A Thesis
Submitted in Partial Fulfillment of the Requirements for the
Masters of Science degree

Department of Physics
In the Graduate School
Southern Illinois University Carbondale
May 2013

THESIS APPROVAL

MANUFACTURING GALLIUM DOPED ZnO THIN FILMS SUITABLE FOR USE IN THIN FILM TRANSISTORS USING UNBALANCED MAGNETRON SPUTTERING

By

Timothy R Jones

A Thesis Submitted in Partial

Fulfillment of the Requirements

for the Degree of

Masters of Science

in the field of Physics

Approved by:

Dr Aldo Migone, Chair

Dr Saikat Talapatra

Dr Thushari Jayasekera

Graduate School
Southern Illinois University Carbondale
March 26th, 2013

AN ABSTRACT OF THE THESIS OF

TIMOTHY RUSSELL JONES, for a Master of Science degree in Physics, presented on March 26th, 2013, at Southern Illinois University at Carbondale

TITLE: MANUFACTURING GALLIUM DOPED ZnO THIN FILMS SUITABLE FOR USE IN THIN FILM TRANSISTORS USING UNBALANCED MAGNETRON SPUTTERING

MAJOR PROFESSOR: Dr. Samir Aouadi

Gallium doped zinc oxide (GZO) thin films were deposited onto Si (100) substrates. Depositions were performed at relatively low temperatures suitable for use in manufacturing thin films on plastic substrates. Substrates were thermally oxidized, and then thin films were deposited via radio frequency (RF) unbalanced magnetron sputtering. ZnO thin films were also sputtered in order to act as a seed layer for growing nanostructures by the hydrothermal method. Sputtering parameters evaluated independently include pressure, gas composition, power, temperature and the presence of an external magnetic field. Scanning electron microscopy (SEM) was performed on hydrothermally produced samples. Sputtered films used to compare sputtering parameters were grown at thicknesses of 33-64 nm as measured by ellipsometry. The GZO sputtering target had a 5% gallium content, which was deposited on the thin films. This was confirmed by X-ray Photoelectron Spectroscopy (XPS). Films were also evaluated using Raman spectroscopy and four-point probe terminal sensing. Using a comparison of the X-ray diffraction (XRD) of the films, it was possible to evaluate the sputtering parameters in order to minimize their crystallite size. It was calculated that the optimum power to apply to the target in order to minimize crystallite size was 128W. Films also minimized crystallite size by several other independent factors, such as not being in the presence of oxygen, being in the presence of

an external magnetic field, being at a higher temperature, or being at a higher pressure during sputtering.

ACKNOWLEDGEMENTS

Several people who helped me in the process of writing this work. The laboratory at the Wright-Patterson Air Force Base was generous enough to allow us the use of their equipment, including their scanning electron microscope, raman spectroscopy, four-point probe, and X-ray photoelectron spectroscopy machine. Clay Watts made hydrothermal substrate holders vital for implementing the hydrothermal growth technique. Ahmed Al-Asadi was also very helpful, in helping with much of the experimental procedure, especially the hydrothermal technique, but also in various cleaning and measuring techniques. However, I want to extend the greatest thanks to D'Arcy and Dr Aouadi. D'Arcy was vital in travelling back and forth to the Air Force Base to do the measurements, performing sputtering depositions, X-ray diffraction and was a very helpful mentor that guided me through the whole process, going above and beyond what anyone could expect from her. And finally, I want to thank Dr Aouadi, who took me on as a student quickly and helped me acclimate to working in the lab. He guided me into unfamiliar subject matter and was very involved in the experimental process by doing many sputter depositions, and also in the realm of ellipsometry, both by training me and taking measurements. Being quite patient with me, he was straightforward and helpful in a complex transition time, and has taken the time to travel between Carbondale, Illinois and Denton, Texas several times for my benefit. I am most grateful to him.

TABLE OF CONTENTS

LIST OF TABLES

LIST OF FIGURES

CHAPTER 1 INTRODUCTION

Screens are widely used in today's society, for computers, TVs, mobile phones and many other devices. One of the most popular types of screen is the LCD (liquid crystal display) screen, whose sales have generate 6.1-7.0 billion dollars per month from January 2012-January 2013[1]. A screen must interface with the switches of the circuits determining what it should display. To use a screen each pixel must be able to be turned on and off. There are two methods for controlling pixels of a screen, by active and passive matrix displays. Passive matrix displays sends a signal to change the pixel, whereas the active matrix continuously sends a signal for which pixels should stay on[2]. Active matrix display is used in most TVs, computers and phones. For switching these signals on and off, each color within each pixel of the screen must have a transistor, usually made by thin film methods and known as a thin film transistor (TFT).

A transistor acts as a current amplifier[3], changing a low current signal into a higher current signal or vice versa. An early application for transistors was first used for transistor radios[4]; they allowed the amplification of energy transmitted through the air as an electromagnetic signal, which signal could be turned into sound. Many applications were immediately apparent, and a symposium on the transistor was hosted by Bell Labs a few months after its discovery. One of these applications was the use of the transistor in computers[5].

Transistor with three terminals:

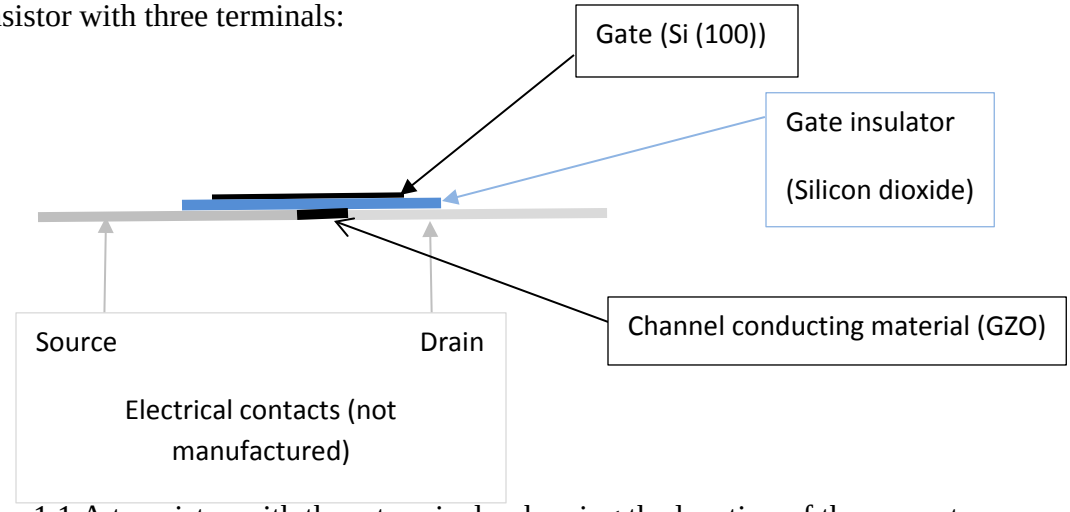

Figure 1.1 A transistor with three terminals, showing the location of the current source, drain, and gate. The use of the three different materials, silicon, silicon dioxide and GZO is also shown. Particular focus will be given to the channel conducting layer, made of GZO.

A basic transistor has four electrical leads: two electrical inputs and two electrical outputs. One input/output pair modifies the current output of the second input/output pair which is at a higher current[6]. Some transistors do not have all four connectors. Often only three are used, with only one low current input regulating the higher output current[6]. The high current input is sometimes called the "source" and the high current output is called the "drain". They are regulated by the lower powered "gate" [6].

Much of the utility of a transistor is due to the fact that it can be used as a switch. Applying an electric field will deplete the charges in a region of the channel, causing the circuit to close[6]. The on and off positions of the circuits translate into the 1s and 0s used in computers

and other digital electronics[6]. Changing these 1s and 0s provide the basis for all operations done in the integrated circuits that make up modern computers[6].

The some transistors work through the field effect. In conductors such as metals there is an abundance of conduction electrons, and in insulators there is an absence of conduction electrons. However, in semiconductors mobile conduction electrons are present. These conduction electrons in semiconductors are present in sparse enough quantities that they can be pushed around within the material. The gate voltage can induce an electric field which pushes the electrons in the conduction channel to close the circuit between the source and gate[6]. The gate, of course, will not be in direct electrical contact with the conduction channel, otherwise it would complete the circuit. Rather, it is slightly insulated from the conduction channel by a gate insulator. When a transistor works in this way, it is called a "field effect transistor" (FET), due to the fact that the electric field is used to change the position of the electrons in the conduction channel[7].

A variation on the normal TFT is a nanowire transistor. In this case, a nanowire lies across a gap between the source and the drain, acting as a conduction channel[8 - 11]. Methods exist [12 - 15] for transferring nanowires from an upright array (perpendicular to the surface of the substrate), to laying down on a substrate.

Most TFTs are made with indium-doped tin oxide (ITO) or fluorine-doped tin oxide (FTO) as the conduction channel. These materials are known for their properties as conducting transparent thin films, but are expensive and rare[16]. Doped zinc oxide offers a cheaper solution. Zinc oxide is most often doped with either gallium or aluminum. Until recently, one of the problems with using GZO for making TFTs for screens was the reduced accuracy with which the

transistors could be delineated, as strong acid etching is less accurate for GZO than for ITO. However, it has recently been shown[17] that using weak acid for etching allows GZO to be etched with the same accuracy as has been shown previously for ITO.

Most defects in the processing of LCD screens are found within the TFTs. A defective transistor will not allow the part of the pixel that it controls to switch on and off properly, eliminating a color from that pixel. As many screens include millions of pixels, even a small percentage of defects on a large screen array can result in several pixels malfunctioning, thus improvements in the quality of the TFT surfaces are important.

This work will attempt to find the optimal sputtering conditions for making a GZO layer. This will be achieved by systematically varying the sputtering parameters. Various sputtering parameters such as temperature, pressure, gas composition, power and an external magnetic may be optimized for making GZO. An external magnetic field has been shown to improve defects at low temperatures for Aluminum-doped ZnO[18]. Changing the pressure of the gas has shown a difference in sputtering as well[19]. Higher temperature sputtering is well-known to result in GZO layers with fewer defects and decreased resistivity[20-21]. A layer with fewer defects could improve the electrical properties of the layer by eliminating voids in the GZO, reducing resistance, and providing a surface with less roughness which could then be more easily and accurately processed. However, all of these parameters have not been optimized for GZO in an external magnetic field. This is important because a magnetic field will increase the flux of the material being deposited on the surface but not increase the power exerted on the ions.

Sputtering has advantages of being much quicker than chemical methods of deposition, as well as being adaptable to roll-to-roll processing. Roll to roll processing is a highly efficient

method of manufacturing where the substrate, typically plastic, is supplied continuously from a roll, and then printed on as the substrate travels through the manufacturing apparatus. We will focus on sputtering of zinc oxide at low temperature that would be suitable for use on plastic substrates such as polyethylene terephthalate (PET). It has been well demonstrated that ZnO becomes more crystalline when sputtered at higher temperatures[20,21] or when it is annealed post-sputtering[22232424]. The difficulty is in reproducing this level of crystallinity at lower temperatures without annealing, since high temperatures would melt the flexible plastic substrate (the melting point of PET is about 260˚C[25]). ZnO has been sputtered on plastic substrates in the past[26], though the low temperature limits its quality. Here ZnO will be sputtered on a silicon substrate in order to test the electrical properties of the film, since silicon is one of the most common materials used for sink and source layers of a transistor[6]. Some have already studied particle sizes of ZnO films on silicon[2728], and others the resistivity of the ZnO films[18-19,29]. Others have even evaluated the thickness, crystal properties and resistivity of GZO samples sputtered in the presence of an external magnetic field[30]. However, these characterizations have not been used to optimize the other sputtering parameters (such as the presence of oxygen, the power level, or the pressure) for sputtering in an external magnetic field. This is what we will undertake here.

Currently, one of the most reliable ways to achieve GZO nanostructures is through the use of a hydrothermal method. However, hydrothermal methods for growing GZO nanostructures on substrates necessitate a ZnO seed layer on the substrate[31]. It will be verified that a sputtered seed layer of ZnO can be used to produce GZO nanostructures with various concentrations of gallium used for doping.

OBJECTIVES

The objective of this work is to find a way to manufacture a conducting channel of a TFT made out of GZO. Towards that end, ZnO doped with 5% gallium will be sputtered with an unbalanced magnetron sputtering machine. Sputtering parameters will be evaluated to minimize the crystallite size of the thin film layer, which will be measured using X-ray diffraction. Sputtering parameters include:

- Temperature
- Presence of an external magnetic field
- Composition of the gases in the sputtering chamber
- High or low pressure in the sputtering chamber
- Power applied to the sputtering target

The thickness of the samples to be compared will be measured to be between 33-63nm using ellipsometry. The thin films will be sputter-deposited on Si (100) substrates, on top of an insulating SiO_2 layer, which will allow resistivity measurements to be made of the top layer by a four-point probe. The composition of the samples will be verified using X-ray photoelectron spectroscopy. On top of some sputtered ZnO samples, hydrothermal growth will be achieved with different concentrations of gallium, and the results will be shown in images taken using a scanning electron microscope (SEM). Using the characterization of the samples, it will be possible to recommend how to manufacture a sputter-deposited 5% GZO thin film for use as a conduction channel in a transparent TFT.

CHAPTER 2 EXPERIMENTAL METHODS

Thin film layers were grown on Si substrates by a variety of methods, including SiO_2 layers by silicon oxidation, and ZnO and GZO layers by unbalanced magnetron sputtering. Nanostructures were also grown using the hydrothermal method. The focus was on characterizing the ZnO and GZO layers generated by sputtering. The layers were characterized in a variety of ways. The thicknesses of layers were found by ellipsometry, images were taken with scanning electron microscopy (SEM), and crystal structure was analyzed by X-ray diffraction (XRD). Composition of the samples was found using X-ray photoelectron spectroscopy (XPS), the molecular bonds analyzed with Raman spectroscopy and electrical resistance found using a four-point probe method.

SAMPLE PRODUCTION

SUBSTRATE PREPARATION

Substrates were prepared from silicon wafers with crystal structure in the (100) direction. They were cut by scoring with a diamond scribe and then breaking them along a ruler's edge, aligning the breaks with the crystal orientation. The silicon pieces that were going to be used as substrates for a hydrothermal process were cut into strips 3.2 cm by 1.3 cm, whereas the silicon pieces used as substrates for sputter-deposited films were usually cut larger, with widths and lengths of around 4-5 cm. After being cut, the silicon was cleaned by sonicating in 100% acetone for 15 minutes, and then in 99% methanol also for 15 minutes. After the sonication the substrates were rinsed in deionized water, and dried with nitrogen gas.

Substrates for the hydrothermal process were masked with scotch tape so that the seed layer would not deposit on the selected region. This region would then be used to hold the substrate during the film growth of the hydrothermal process.

SILICON OXIDATION

An oxide layer can be grown on the top of a substrate by annealing. Thermal growth of silicon oxide typically occurs by one of two reactions, either due to the presence of oxygen or the presence of water. These reactions are:

$Si+O_2->SiO_2$

and

$Si+2H_2O->SiO_2+2H_2$ [32]

There are well known equations governing the growth rate for either of these reactions (known as the Deal-Grove model[32]). However, growth rate is more difficult to calculate when both reactions occur simultaneously.

An oxide layer was not grown on substrates that were to undergo the hydrothermal process. To oxidize the surface of the silicon, non-hydrothermal samples were arranged on a ceramic plate. Dust particles from the furnace insulation of the furnace were vacuumed out of the Barnstead Thermolyne FB 1400 furnace, if necessary. The front edge of the ceramic plate was placed about half a cm from the front of the furnace. The thermostat on the furnace was set to 1070˚C. The furnace reached 1000˚C in about 50 minutes. When the temperature of the furnace reached 1050˚C, the set temperature of the furnace was decreased to 1050˚C, and a timer started. After a set amount of time (depending on the thicknesses of previous oxidation layers),

the furnace was turned off and allowed to cool overnight. The samples were then extracted at room temperature and the thickness of the oxide layer was measured by ellipsometry.

SPUTTERING PROCESS

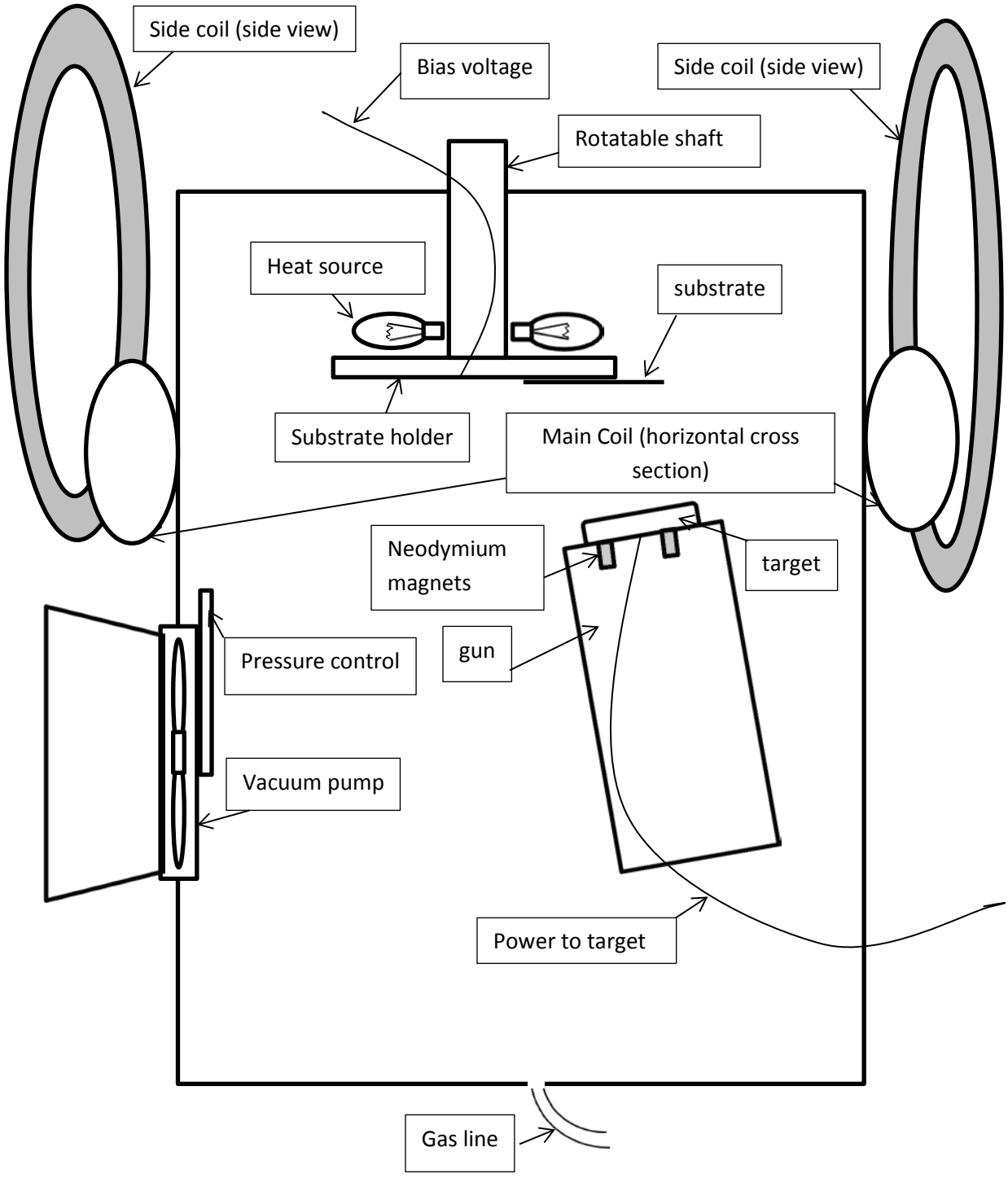

Figure 2.1 Components of sputtering apparatus

Substrates were sputtered using an unbalanced magnetron sputtering apparatus. Sputter deposition occurs when a plasma is created using an electrical potential which is generated between a source material (called the target) and the rest of the chamber. This potential strips the electrons from the gas, ionizing it near the target's surface. The particles in this gas bombard the surface of the target, releasing material from the target which then deposits onto the substrate. Permanent magnets are mounted behind the target, which concentrate the ionized gas near the target to gather more material before it gets deposited onto the substrate. Sometimes a potential (called a bias) is also generated behind the substrate in order to concentrate plasma there as well. The environment in which this plasma is generated may be controlled by the pressure, the temperature, and the composition of the gases it contains. A magnetic field imposed on the sputtering environment can promote a high flux of low energy ions[33]. This high flux of low energy ions should favor formation of a crystal structure based on the crystal structure of the substrate and its binding energies rather than a more amorphous growth based upon the more forceful bombardment of the plasma.

After an oxide film was deposited (or, in the case of the hydrothermal samples, once the substrates were masked), the samples were placed into a sputtering machine, nicknamed “Maggie”, manufactured by AJA International Inc. To place the samples inside, the samples were first attached to a substrate holder. If the sputtering was carried out at room temperature, the substrates were simply affixed with double sided copper tape. If the substrate was to be heated, it was glued to a substrate holder with conductive silver paste (commonly used for gluing samples in microscopy). After letting the paste dry for at least 2 hours under a 2kg weight, any extra paste was cleaned off with acetone. Samples for which a magnetic coil was going to be used were glued off center on the substrate holder so they would be closer to the plasma plume

inside the machine. Once the samples were in place, the sample holder was inserted into the machine (by way of a pressure load lock), with the sample facing down, and depressurized. The substrate was heated to 100˚C. Samples not positioned off-center, as mentioned above, would be rotated continuously, a full turn every few seconds, for a more even coating. The pressure inside the machine would be at least as low as 7×10^{-7} Torr, to minimize the amount of contamination during sputtering. After pumping down, gases were introduced at specific flow rates, and the total pressure of the system adjusted by partially closing off the exit where a pump was evacuating the chamber. This would regulate pressure on the order of a few mtorr. After that, a magnetic field of 68.0 gauss was created near the substrate holder by coils around the machine. One main horizontal coil exerted most of the field (about 59 gauss as measured by an FW Bell Gauss/Tesla meter model 14048) with over 9¼ amps pushed through about 200 coils 45 cm in diameter using a high voltage power supply, whereas two other coils (also about 45cm in diameter which had 68 coils each) provided 14 gauss to the substrate when both on together, focusing the plume from the sides with 13.1 amps provided for each by switching power supplies. Inside the chamber, a metal flap called a shutter separated the target from the substrate until the sputtering was to begin, at which time it would open. Before this, a potential would be created on the target by a power supply, and in some cases an additional switching potential would be created from behind the substrate, referred to as a "bias". This potential from the substrate was part of the reason for using copper tape or silver paste, since they are highly conductive and would ensure that the potential applied to the substrate holder was also transferred to the substrate itself. Sometimes the switching potential would be used behind the target instead of the substrate, in which case the substrate would not have a bias. The switching of the power supply is in the radio frequency portion of the spectrum (13.56 MHz), and thus this

is referred to as RF as opposed to DC magnetron sputtering which uses a non-switching power supply. So, once the gases are introduced into the chamber and the coils creating the magnetic fields are turned on, then the potential difference is switched on, and the sputtering timed from the moment that the shutter opens (a metal flap shielding the plasma generated by the target from the substrate).

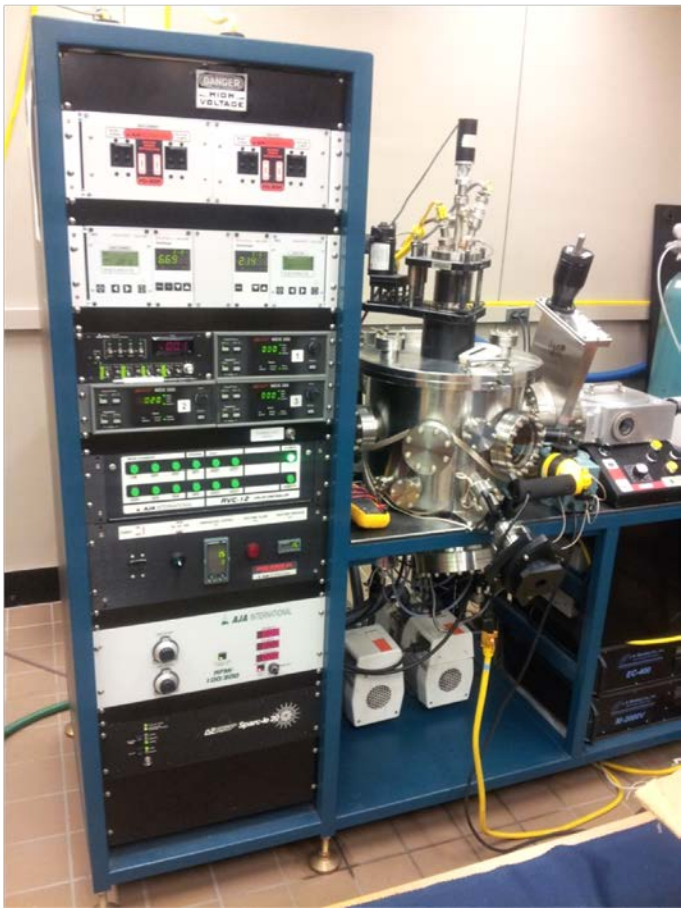

Figure 2.2 The unbalanced magnetron sputtering machine used for most of the depositions, colloquially known as “Maggie”.

For the seed layers of the hydrothermal samples and some preliminary DC ZnO sputtered films were produced in another apparatus ("Lucy"), similar to the machine described above, except that the substrates were not suspended, but were placed on a platform on top of the substrate holder with the plasma being deposited from the top. Deposition conditions such as bias, target RF and DC, control of pressure, temperature, gases present in the system were kept the same.

HYDROTHERMAL PROCESS

Hydrothermal synthesis is a name given to a variety of processes that were discovered by researchers attempting to mimic the geological conditions of the earth[34]. These processes typically require high temperatures and pressures, and may be used to produce a variety of different crystals, depending on the composition and conditions of the experiment. Hydrothermal processes often require the use of autoclaves, and are used to make a variety of gemstones in the lab. L Vassiers was the first to make ZnO nanowires in a the laboratory setting through this approach[35]. The growth of these wires occurs at quite a low temperature and pressure for a hydrothermal reaction, at just 100˚ C near atmospheric pressure.

Hydrothermal synthesis of zinc oxide nanowires follows a group of chemical reactions. When a 1:1 molar ratio of hexamethylenetetramine is added to zinc nitrate in an aqueous solution, the following reactions occur:

$(CH_2)_6N_4+H_2O->6HCHO+4NH_3$

$NH_3+H_2O->NH_4^+ +OH^-$ [36]

Hexamethylenetetramine dissociates into formaldehyde and ammonia in water. The ammonia ionizes in the water to create hydroxide anions. These reactions can provide a pH buffer for the other reactions.[36] Zinc nitrate will ionize in water:

$Zn(NO_3)_2 \rightarrow Zn^{2+} + 2NO_3^-$

The NO_3^- ion will form some sort of salt with another ion, likely NH_4^+, but neither will be pertinent to the actual oxidation of the zinc oxide:

$2OH^- + Zn^{2+} \rightarrow Zn(OH)_2$

$Zn(OH)_2 \rightarrow ZnO + H_2O$ [36]

The base stabilizes into ZnO and H_2O. Thus ZnO is formed from zinc nitrate ($Zn(NO3)_2$) and hexamethylenetetramine ($(CH_2)_6NH_4$) in water. The zinc oxide formed is usually hexagonal in shape. Zinc oxide is usually wurtzite in structure, made up of tetrahedral groupings which pack together forming a hexagonal structure[35]. Since this structure does not have symmetry along all of the cubic axes, this structure provides the opportunity for growth along one axis, so that nanowires can be created.[35]

To synthesize hydrothermal zinc oxide, the lab oven was first preheated to 100˚ C. 0.280g of hexamethylenetetramine (HMT) was measured out onto a zeroed boat, and added to 80ml water. This solution was stirred on a stirring plate. Meanwhile 0.595g of Zinc nitrate hexahydrate was measured onto a zeroed boat, and also added to 80ml water. This was also stirred with a stirring plate. The two solutions were combined and stirred for 10-20 minutes. The pH meter was calibrated (by solutions with pH of 4.00, 10.00 and 7.00). The pH of the solution was checked, and adjusted if it outside the 6-7 range using 1M HCl and 1M NaOH.

Cleaned substrates with a seed layer of about 40nm (this is the optimal thickness for ZnO nanowires[37]) were put into slots of holders made out of polytetrafluoroethylene (PTFE) at the bottom of a beaker. The solution was added to the beaker, and the top of the beaker was sealed airtight with aluminum foil and electrical tape. The beaker was set in the oven for 8 hours. After this time, the samples were rinsed with nanopure (18Ω) water, and air dried.

SAMPLE CHARACTERIZATION

ELLIPSOMETRY

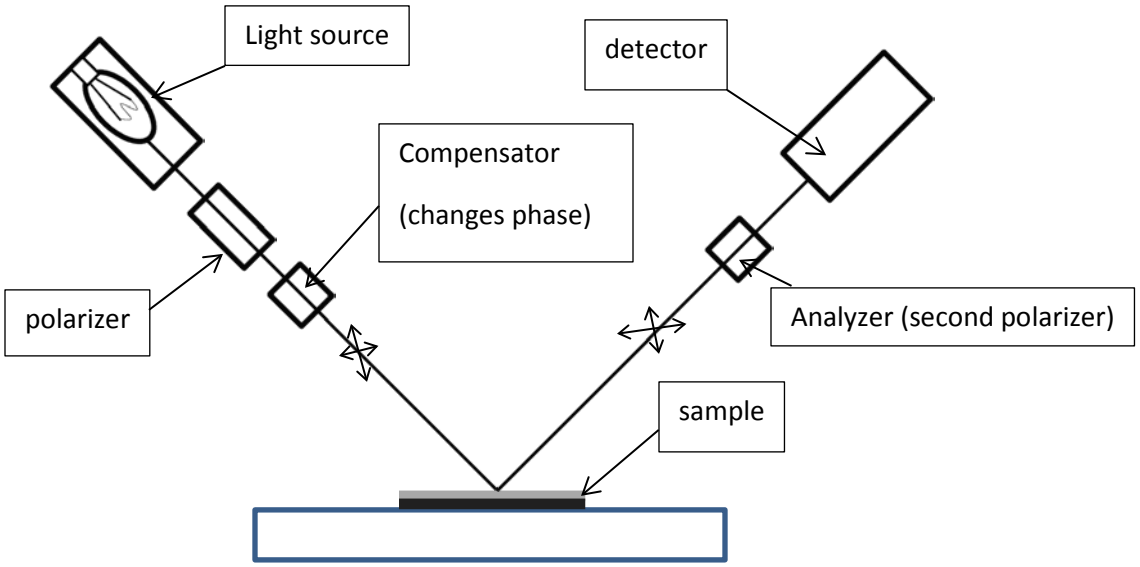

Figure 2.3 Components of the ellipsometer

To analyze the samples, the thickness was measured using spectroscopic ellipsometry. An ellipsometer measures the polarization of light. However, rather than measure an exact polarization value, ellipsometry measures the ratio of the polarization, called the "complex reflectance ratio", ρ. In other words, $\rho=r_p/r_s$, where r_p is the polarization perpendicular to the

sample and r_s is the polarization parallel to the sample. The complex reflectance ratio, ρ, is given by:

$$\rho=\tan(\Psi)\, e^{i\Delta}$$

where tan(Ψ) is the ratio of amplitude reflection and Δ is the phase shift, since these are the real and imaginary parts of ρ. Both of these real and imaginary parts of ρ are detected for a range of energies. The resulting data can be fitted to the thickness of the film, using data which have previously provided films of known thickness as a starting point for modeling thickness. This technique is not suitable to determine the thickness of optically opaque films.

Figure 2.4 The ellipsometer

Ellipsometry was used to measure the silicon dioxide layer prior to sputtering, and then later was used to measure both the thickness of the zinc oxide layer and the thickness of silicon dioxide layer at once. Cauchy oscillators were used to model the optical properties of ZnO[38]. The index of refraction for a Cauchy oscillator model is given by:

$n(\lambda)=B+C/\lambda^2$

$k(\lambda)=0$ [38]

Here n is the index of refraction, B and C are material parameters, λ is the wavelength and k is the wavenumber. These functions are used to fit to a dielectric function using a least-squares iteration procedure, from which it is possible to derive the thickness. The dielectric function is not easy to calculate directly from the ellipsometry measurements in this case[39], so fitting using iterations was used. Iterations were performed with the WVASE 3.74 software using a least-squares method (the damped least-squares method of Levenberg-Marquardt) which iterates to minimize the gradient of the area of the squares after starting with an initial guess. Silicon dioxide was fit according to published SiO_2 data[40] before sputtering. After sputtering, the mean squared error value was minimized for the trend found when both layers were modeled at once. No measurable optical differences were found due to Gallium doping. For uneven ZnO coatings using the magnetic coil, the thickness at the thickest part of the coating was measured, where X-ray diffraction was also performed.

X-RAY DIFFRACTION

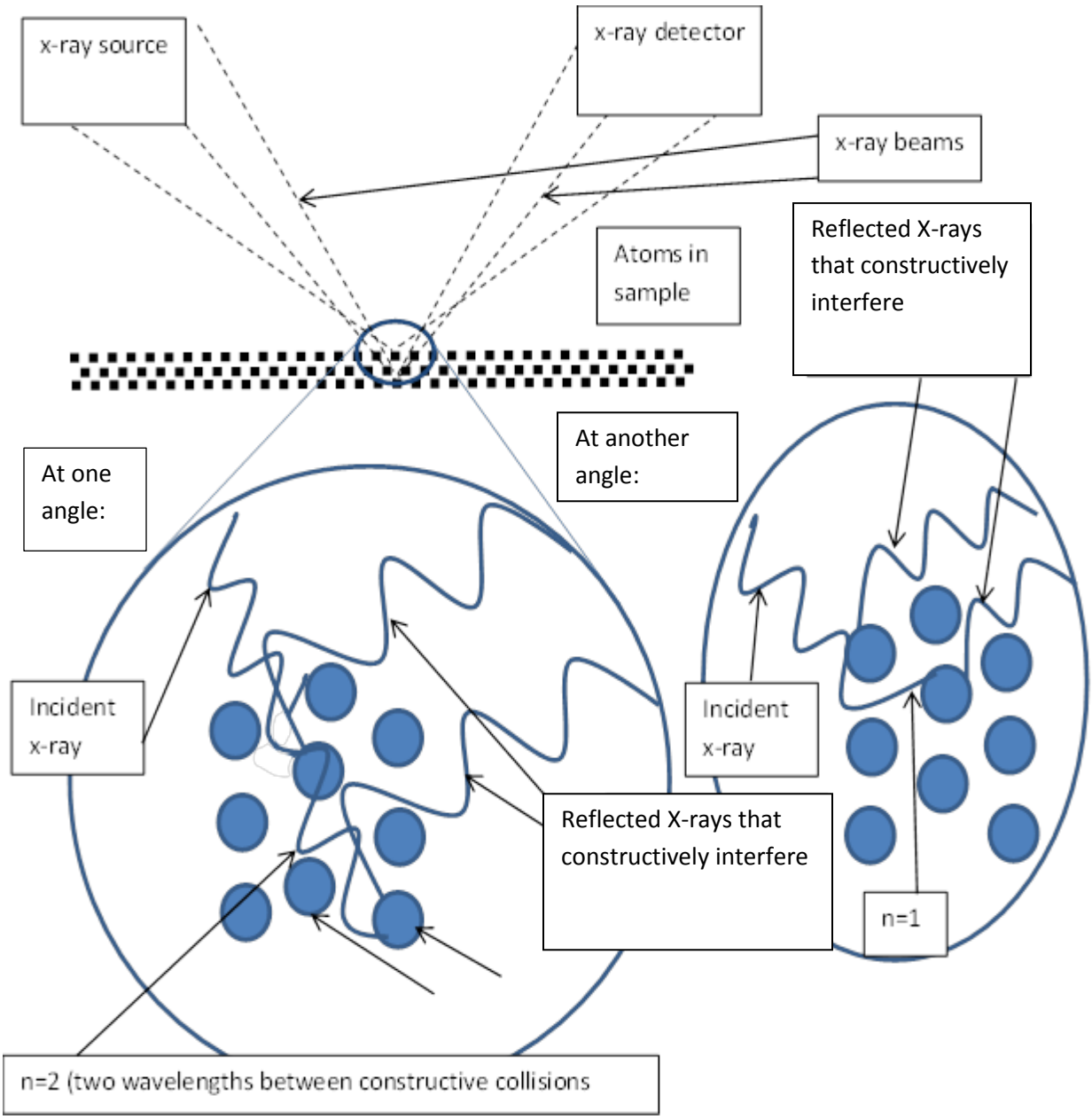

Figure 2.5 X-ray diffraction

X-Ray diffraction works by subjecting the substrate to X-ray radiation, and detecting at what angles the beam is reflected. This detects the energies of the reflected X-rays based on Bragg's Law:

$n\lambda=2d\sin\theta$

Here λ is the wavelength (which will be 0.15418 nm since the source of the X-ray is standard, the Cu Kα -rays), θ the angle the X-ray is incident to the substrate (the total deflection is 2θ), d is the spacing between the planes of the crystal lattice, and n is an integer. If the X-rays hit particles in adjacent planes, in order to combine constructively, the extra distance to that farther plane will have to be an integer "n" number of wavelengths away. Through this interference pattern formed we can obtain some idea of the quality of the crystal structure of the film. A crystal structure with fewer defects will have a stronger interference and result in a smaller spot. The quality can be found by the Scherrer equation, which shows how large the ordered domains of the crystal are. The Scherrer equation is:

$\tau=K\lambda/(\beta\cos\theta)$

Here λ and θ are the same as in the Bragg equation, β is the width of the interference peak at its mean height (also known as the full width at half maximum (FWHM)), and K is a constant known as the "shape factor", which is equal to 0.94[41]. These combine to compute τ, the size of the crystal domains. τ can be larger than the value computed by this equation in some circumstances, for instance if the sample was under strain when measured.

SCANNING ELECTRON MICROSCOPE (SEM)

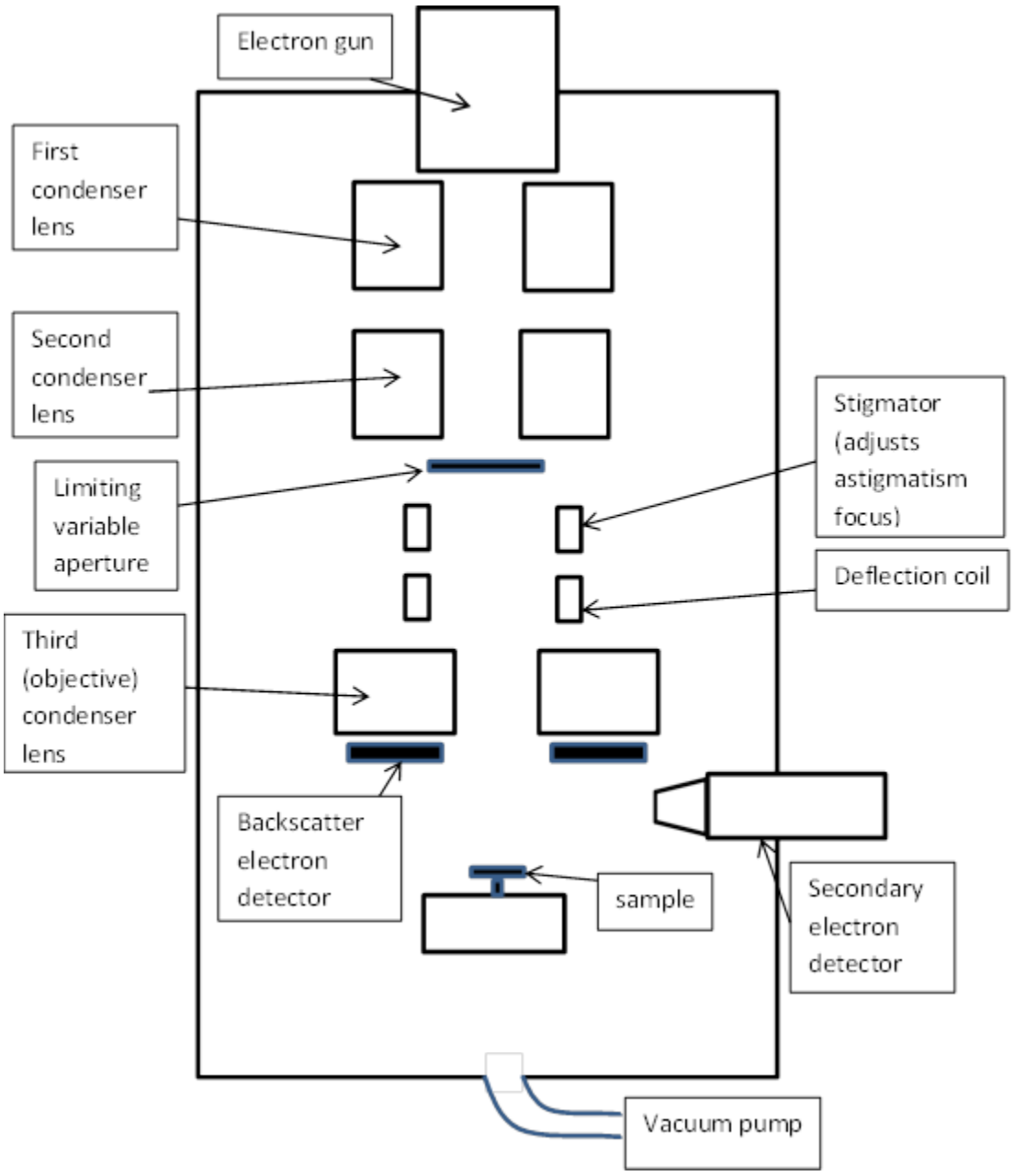

Figure 2.6 Scanning electron microscope

Some samples were inspected using a Scanning Electron Microscope, which allowed detection of nanowires. In scanning electron microscopy, a sample with a conductive upper layer is put in an evacuated chamber. An electron beam is aimed towards the sample. This electron beam is focused two times by lenses, sometimes called “condenser lenses”. Some of the beam is blocked depending on the setting for the variable aperture. The beam is further focused by electromagnetic coils, sometimes called “deflection coils”, one of which is the stigmator, which corrects for astigmatism. A third condenser lens then focuses the beam to a smaller area. The highly focused beam hits the substrate and scatters off the surface. This back-scattering from the electron beam is measured in order to produce a picture. Because the electrons originate at from the surface of the sample, it is important for the surface to be conductive. Non-conductive samples must be sputtered with very thin gold (a few angstroms thick).

X-RAY PHOTOELECTRON SPECTROSCOPY (XPS)

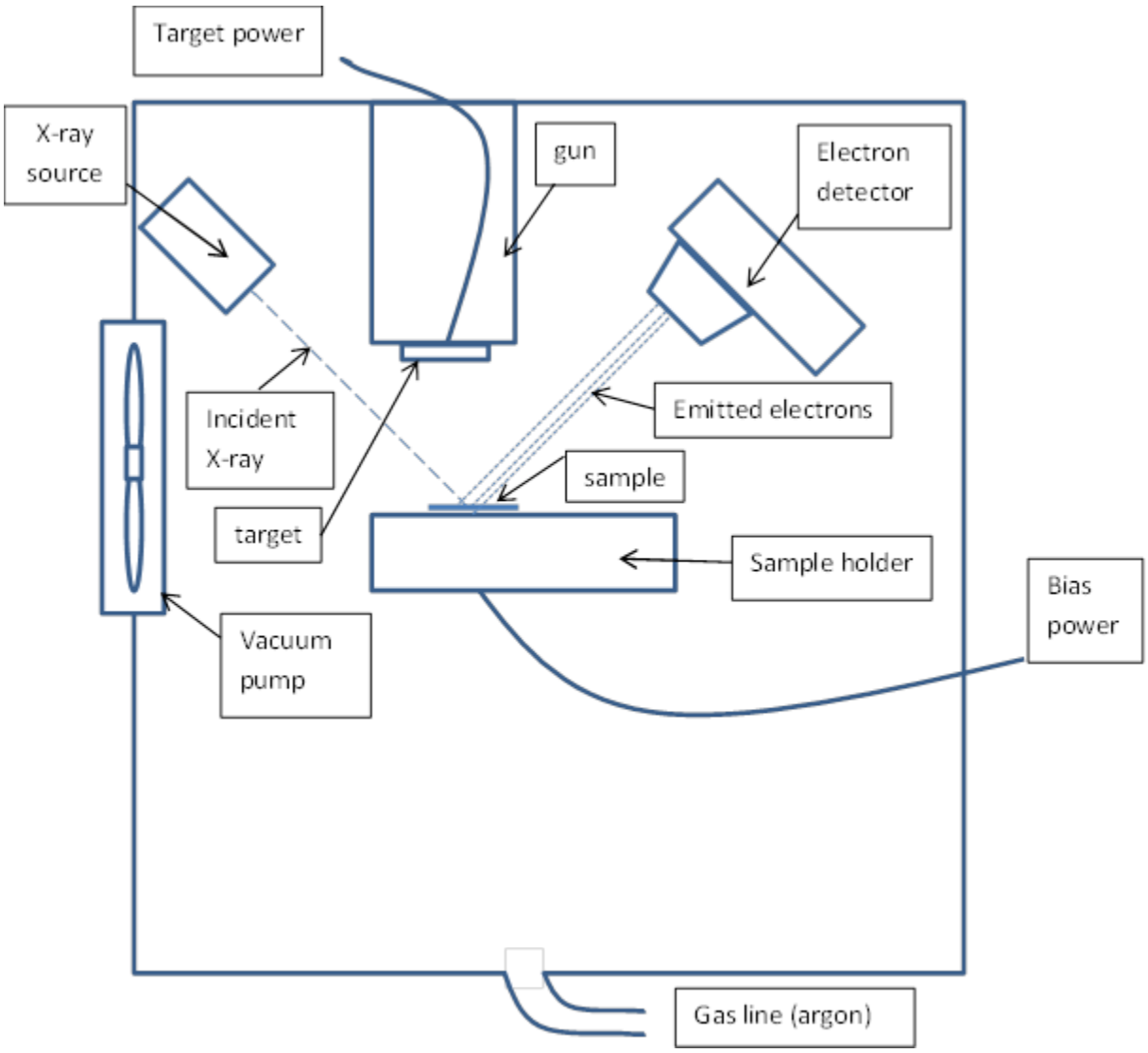

Figure 2.7 X-Ray photoelectron spectroscopy

For XPS, a sample is bombarded with X-rays. To do this, the sample put into vacuum and gases can be introduced as in sputtering. The X-rays that penetrate into the interior of the sample are usually captured by the sample. Only electrons that interact with the very top surface

reflect back, and their energies measured in a detector. Because it only detects the surface, an ion beam is present. It can remove any oxidation or contaminates on the surface. The binding energy can be found from the energy of the initial electrons, that of detected electrons and a work function Φ_s (a known energy the electrons exert on the machine):

$$E_{binding}=E_{source}-E_{detected}-\Phi_s$$

Those binding energies provide the composition of the material. From this it was possible to get an estimate for the gallium content in the sputtered films, as well as an estimate of oxygen deficiency within the film. However, these values for surface oxygen may be different from the oxygen in the interior of the film.

RAMAN SPECTROSCOPY

Raman measures the strength of molecular bonds at the surface of a material. In Raman spectroscopy, a light source of a given energy shines on the sample and is scattered off. The light exerts the energy on a bond between two atoms either by moving one of the two nuclei at the end of the bond, or by changing the position of the electrons connecting the nuclei. When the light exerts energy on the nucleus, it is called “Stokes scattering” and when it absorbs energy from the bond the same way it is called “anti-Stokes scattering”, both of which are inelastic. Motion of the electrons is Rayleigh scattering, which is elastic. The difference between the energy of the incident and scattered light is measured. Certain amounts of energy will induce resonance. The amount of energy needed will depend on the length of the bond and the atomic masses.

The light source for the Raman spectroscopy was a 300 mW 532 nm laser. Rayleigh scattering was filtered out, and only Stokes and anti-Stokes scattering measured. The intensity of

the light was output as a function of "Raman shift". Raman shift is the difference between the inverse wavelengths, often noted in cm^{-1}: $\Delta w=(1/\lambda_0-1/\lambda_1)$ where λ_0 is the wavelength of the light source and λ_1 is the wavelength detected.

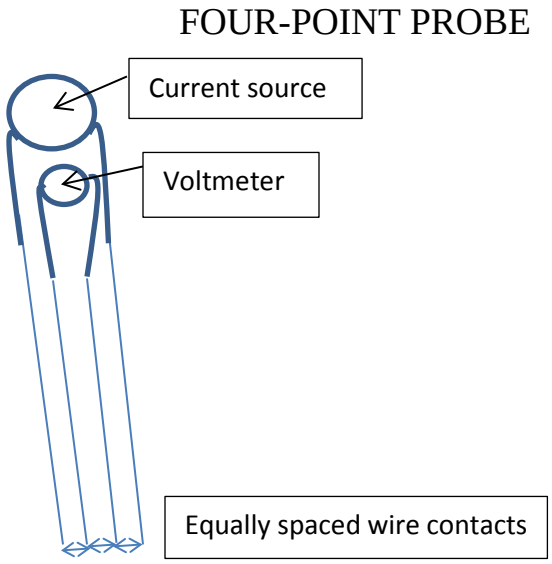

Figure 2.8 Four-point probe

Using a normal two-lead potentiometer to measure resistance on the conduction channel might cause the charges to migrate, as the potential applied through the leads might act to change the location of the conduction electrons. Instead, a four point probe is used, with minimal current applied to an entirely different place on the substrate so as not to disturb the mobile charges in the layer. A four point probe measures the electrical resistivity. It has 4 probes each 1 mm from the next, positioned collinearly. The two at the end provide a test current, while the two in the middle measure the response of the material due to that current. Since different wires provide the test current and measure the resistance of the material, a four point probe measures smaller and more precise resistivities. A four point probe will measure the sheet resistance in

terms of ohms per square length (which units are used for the length are unimportant, only that the measurement is done on the diagonal of a square). Here the sheet resistance is $\rho_{\square}=V\pi/(I\ln 2)$, and bulk resistivity may be calculated by multiplying the sheet resistance by the thickness of the film, assuming (as will be the case) that the film is much thinner than the distance between the probes.

CHAPTER 3 RESULTS

ELLIPSOMETRY

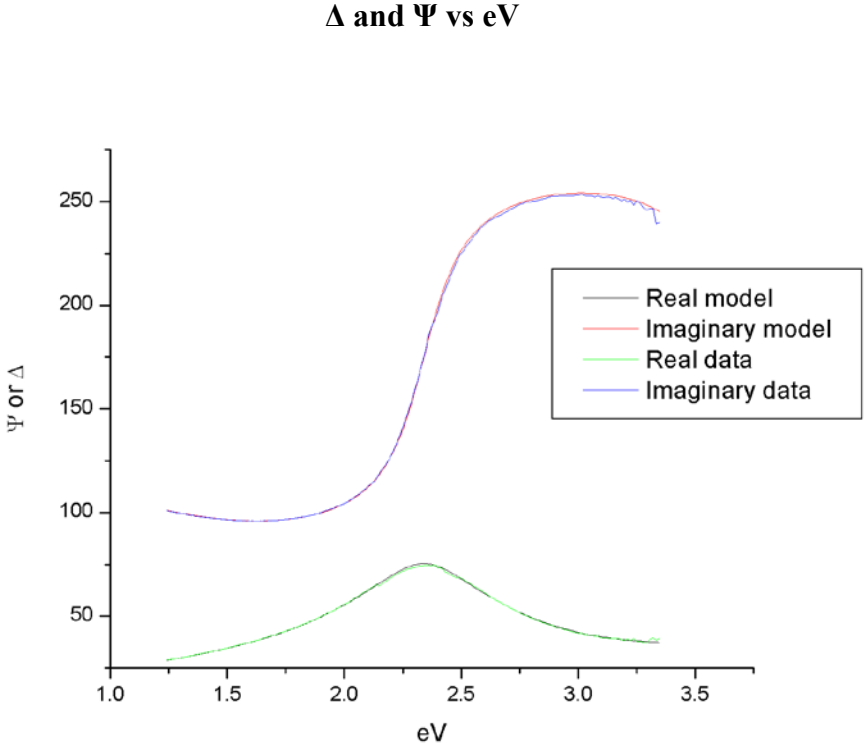

Figure 3.1: Real and imaginary ellipsometric data fitted for SiO_2 on Si for a model of thickness 114.2 nm.

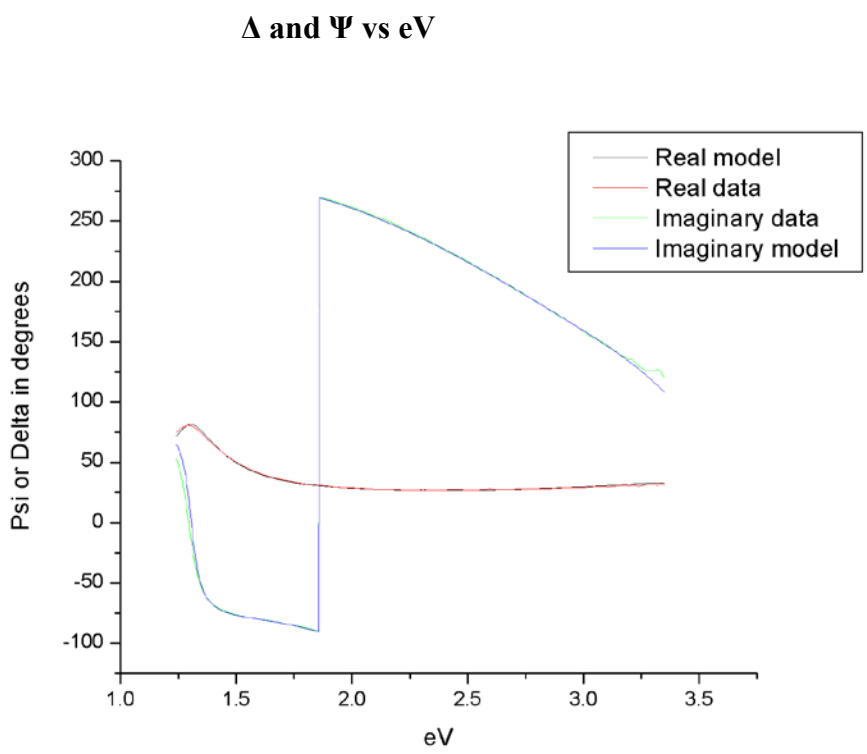

Figure 3.2: Ellipsometric data for the same sample (M28) after being sputtered with GZO. Model of the second graph is generated using thicknesses of 111.7nm SiO2 and 50.7nm GZO.

Graphs such as figures 3.1 and 3.2 were fit for each sample to find all the thicknesses shown in table 3.1. The accuracy of the SiO_2 thickness varies, as seen by the different values in the models above. This is not so much due to the ellipsometry measurements, since the fitting is quite good, but because there is a thickness gradient across the sample. The thickness of the SiO_2 layer varied by as much as 30 nm over the course of a 10 cm long distance between spots as they had been placed inside in the furnace.

Thicknesses for ZnO and GZO were quite consistent across the substrate in earlier samples. This is due to the fact that the substrate was rotating and the plasma was more

dispersed and uniform. However, for the later samples, where the coil was turned on, the samples were no longer rotated. This was due to the fact that the plasma plume when the coil was turned on was much more focused but also off-center, so rotation would have effectively turned the deposition off as the sample moved away from the plume. The thickness of the ZnO layer was measured at the position where the plasma had been most focused upon. Sputtering times were adjusted based upon thicknesses of previous sputterings so that most samples had a thickness around 50 nm.

X-RAY PHOTOELECTRON SPECTROSCOPY

Sample name	Zn:O
L1	53:47
L3	48:52
L5	44:56
L9	51:49
M1	35:65
M2	50:50
M3	50:50
M9	12:88

Table 3.1: Oxygen composition for undoped sputtered samples. L and M denote which sputtering system was used (machines "Lucy" and "Maggie" mentioned earlier in the experimental section). Lucy was a sputter-down system, while Maggie was sputter-up.

The relative atomic ratios of Zn:O for some undoped films are shown in table 3.3. To see what error was present, the top surface of L1 was etched, and then the composition measured again. A second measurement yielded 53.7:46.2. Either the composition is quite non-uniform, or there is an error of at least 1.5%. Most samples measured were roughly equal in their ratio of Zn and O atoms, but not samples M1 and M9. M9 was glued to the substrate with silver paste,

so it may have been heated (out of the chamber, in atmospheric conditions in the presence of oxygen) for a short time post-sputtering to remove the paste attaching it to the substrate holder, which could have caused additional oxidation. However, M2 and M3 were also attached to the substrate holder in this manner, so this is most likely not the sole cause. The cause of M1's greater imbalance of oxygen to zinc atoms is not clear.

Sample name	% Ga
M4	3.7
M6	5.4
M10	6.3
M12	5.2
M13	5.9

Table 3.2 Percent gallium composition for sputtered samples

The target used for sputtering GZO was 5% gallium. Table 3.4 shows a certain amount of variation in the composition as measured from XPS. The low amount of gallium in the first sample could be due to the sample being composed in part by the oxygen in the chamber and not just the materials in the target, which would decrease the gallium composition. The others had consistently slightly more than 5% gallium, suggesting that the target was slightly more gallium-rich than supposed. The variation is comparable to that in the etched sample. There was no

noticeable inhomogeneity in the gallium target could be seen, even though there was a dramatic color difference between the 5% gallium target (black) and a regular ZnO target (yellow).

	Zn:O ratio	% Ga added	% Ga measured
HT1	42:58	0%	0
HT2	42:57	0.5%	0
HT3	49:51	0.99%	0
HT4	18:77	2.44%	2.2
HT5	40:56	4.76%	3.9
HT6	34:62	2.5%	4.5
HT7	27:68	5.0%	5.2

Table 3.3 Composition of hydrothermal samples

The hydrothermal samples were grown chemically. Their composition is shown in table 3.5. The composition of the first few samples must have been too small to detect. The table indicates an anomalously low gallium composition for HT6, but the gallium composition of the rest of the samples roughly match their intended composition. Table 3.4, table 3.3 and the measurement from the etched sample each suggest that the composition measured by XPS was not terribly accurate, and some variation of ± 1-2%, which is significant since Ga is making up only up to 5% of the composition.

X-RAY DIFFRACTION

X-ray diffraction was performed on samples. X-ray diffraction confirmed the presence of ZnO and Si. Peaks in X-ray diffraction scans from 20˚-60˚ corresponded to X-ray source energies, ka1 or ka2, ZnO or the silicon (100) substrate. The principal ZnO peak was at 34.42˚, corresponding to the (0001) hexagonal orientation. Also visible in some X-ray diffraction data are strong small peaks at around 33.5˚ due to the silicon substrate. Two samples did not follow this pattern, M7 and M29. Ellipsometry showed that the M7 layer was quite thin, about 7.5nm, which was to be expected for a 6 minute run with power at only 50W. It is possible that the M7 layer was sufficiently amorphous and thin to not generate enough constructive interference to be distinguished from noise. The absence of the M29 peak is unexplained, as the ellipsometry showed a 64.6nm layer

The size of the crystallites in the film was measured using Scherrer's formula. A smaller crystallite size corresponds to a less amorphous structure and fewer "islands" formed while sputtering. SEM was also able to spot defects in the films, but these defects were likely due to normal environmental contaminants as opposed to defects in the bulk material. All SEM pictures of the thin films had a resolution lower than the crystallite size found from Scherrer's formula using the length of the full width of the peak at half of its maximum (FWHM values). FWHM values put defect sizes at 0.08-1.24nm. However, comparisons between FWHM computed crystallite sizes of different samples did not show consistent changes with changing manufacturing parameters. Computing the crystallite size using Scherrer's formula and the integral breadth method does not get a definite size scale, as the integral is in terms of degrees and an equipment-specific unit of counts which indicates intensity. The unit is thus an un-

normalized length. However, comparisons between samples yielded more consistent trends. It is unclear why the FWHM calculations varied so differently from the integral breadth method.

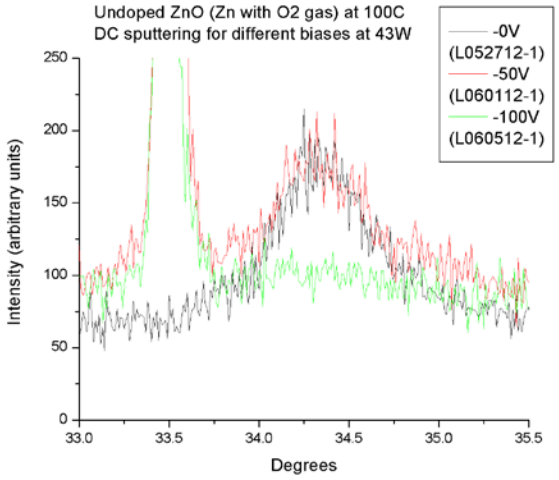

Figure 3.3 Comparison of the effect of an applied bias voltage for undoped ZnO films

Taking the areas of the peaks in figure 3.6, it can be calculated that without a bias, ZnO had a crystallite size of 0.25, which increased to 1.24 for the sample with a bias of -50V. A size of 2.7 was measured for the crystallite size of the sample made with a -100V bias. There is a slight trend here, as the sample without bias had much smaller crystallites, especially since its peak begins so much lower than the others, and the sample made with a -100V bias had essentially no peak at all other than the one at 33.5 due to the Si substrate. Part of the difference for the sample that had no bias applied could be due to a difference in thickness, since the thickness for the-0V sample was 63.6, the -50V was 45.2, and the -100 was 44.7, however the other two samples corroborate the trend of the bias increasing the crystallite size.

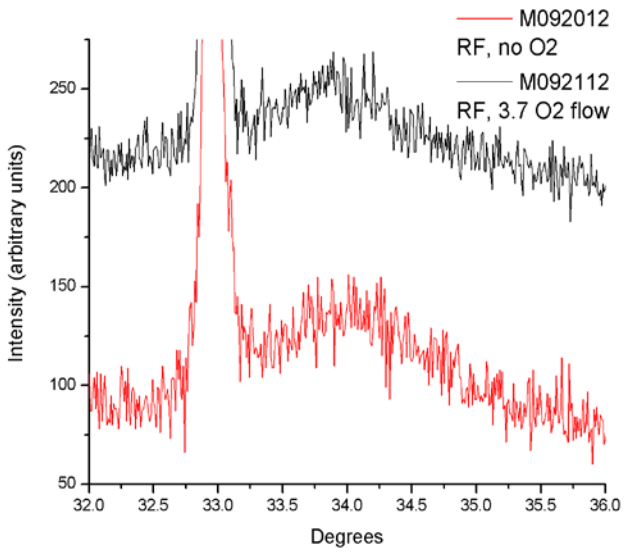

Figure 3.4 Sputtering with and without oxygen at 200 W RF and 100˚ C in a 15 mtorr environment with an external magnetic field

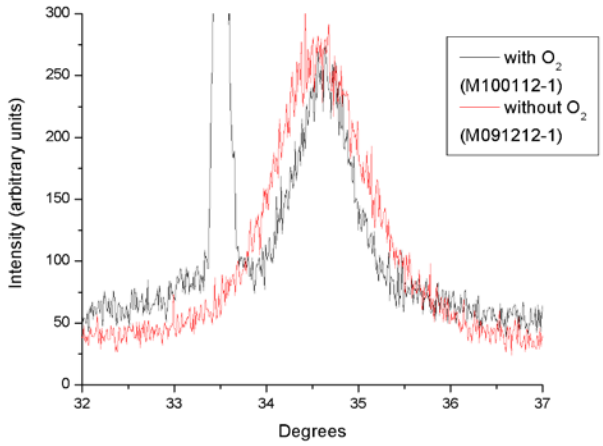

Figure 3.5 Sputtering with and without oxygen at 150W RF and 100˚ C in a 15mtorr environment with an external magnetic field

Figure 3.7 and 3.8 demonstrate that films had smaller crystallite size with no extra oxygen added to the chamber. In figure 3.7 crystallite size as measured from integral breadth was 0.27 for the sample with O_2 flow and 0.20 for the one without O_2 flow (units for particle size are arbitrary though they scale with length). Both samples were sputtered at 200W with RF power in a 100˚ C 15 mtorr environment. The film made without O_2 was 48.0 nm thick, and the one made with O_2 was 59.1 nm thick. In figure 3.9 compares two samples sputtered at 150W with RF power at 15 mtorr and 100˚C. The sample for which oxygen was not used was 47.8 nm thick, while the sample where oxygen was used was 50.7 nm thick. Crystallite size from integral breadth for the sample with O_2 was 0.23, whereas the sample without had a particle size of 0.069. Based on these graphs, smaller crystallite sizes should be achieved with no oxygen added to the chamber, the oxygen coming only from the chemical composition of the target.

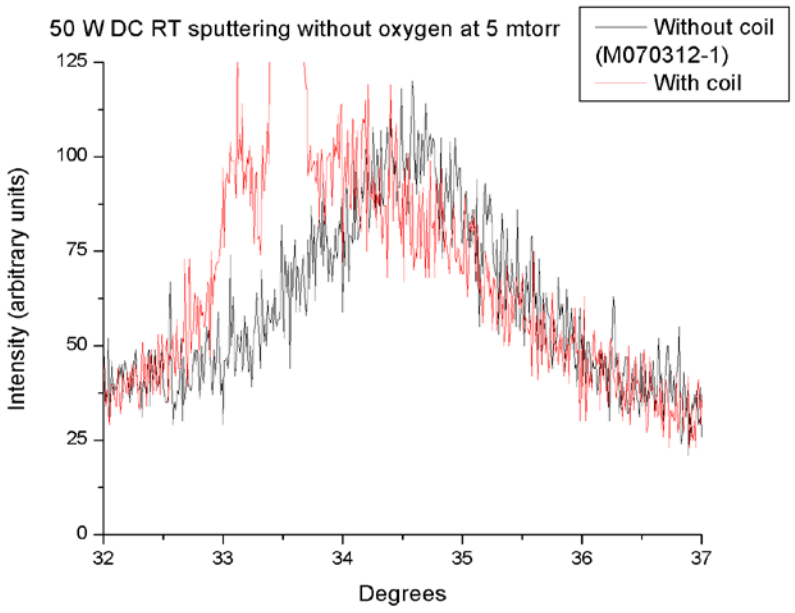

Figure 3.6 Sputtering at 50W DC at room temperature without oxygen at 5 mtorr with and without an electromagnetic coil providing an external magnetic field

The two samples shown in figure 3.9 were made at room temperature using 50 W RF power at 5 mtorr without oxygen in the chamber. The presence of a coil slightly increases the width and area of the peak, indicating a decreased crystallite size. The evidence for this is slightly blurred by the presence of the peak detecting the silicon substrate in the case of the sample where the coil was used. The particle size is 0.20 without the coil and 0.15 with the coil. The sample made with the coil was 51.8 nm thick, whereas the sample made without was 47.5 nm thick. Based on this graph, a smaller crystallite size will come from the use of the coils to apply this magnetic field.

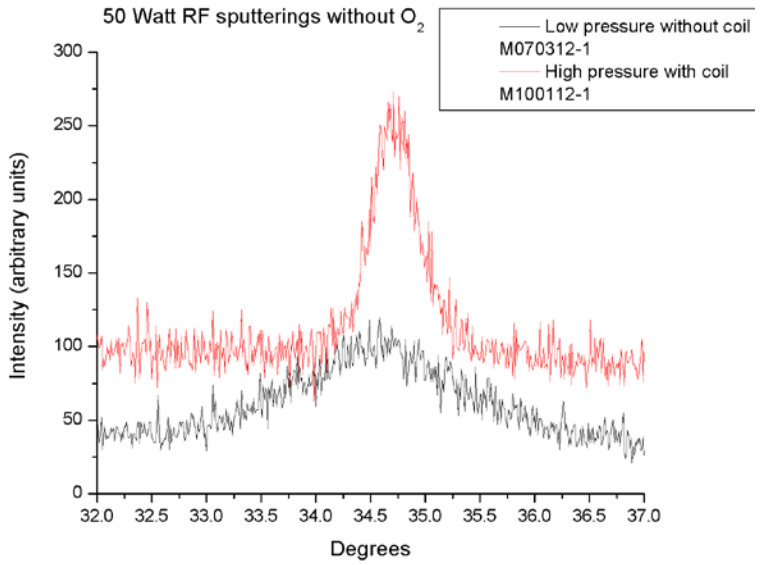

Figure 3.7 The same sample that was made without a coil compared to a sample made at a higher pressure (15mtorr) with an external magnetic coil. The difference is much more dramatic than before, showing the difference that sputtering at higher pressure makes.

In figure 3.10, the sample at high pressure with a coil was 50.7nm thick, whereas the sample without a coil at low pressure was 47.5 nm. The area under the curves is quite similar.

There is much more error inherent in the low pressure measurement, due to the noise making it more unclear where to choose the limits of integration. In this case the high pressure with coil crystallite size was 0.22 and the low pressure without coil size was 0.20. The low pressure sputtering without the coil was done with rotation whereas the high pressure sputtering with the coil was done without rotation, which probably caused a more even coating on the substrate, however this was ignored due to their similar thicknesses. It is apparent that using an external magnetic field with a higher pressure sputtering provides a much smaller crystallite size, since the peak is much larger. The difference between the two methods is somewhat masked in the integral breadth crystallite size value due to the wider but less intense peak found at low pressure without a coil.

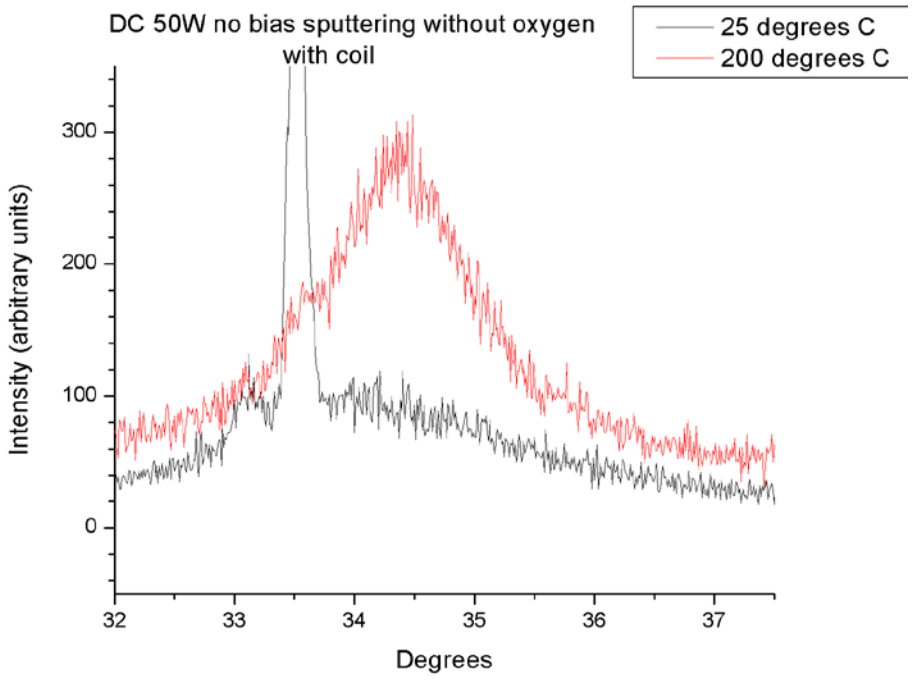

Figure 3.8 Effect of increased temperature

Increasing the temperature decreased the crystallite size. This has been well-documented (cite). Thermodynamic excitation allows particles to move out of positions that cause defects to make the crystal structure more ordered. This graph shows two undoped samples made with DC power. The sample made at high temperature was 39.0 nm thick, whereas the sample made at room temperature was 51.8 nm thick. Crystallites at low temperature were 0.15 whereas those at high temperature were 0.079.

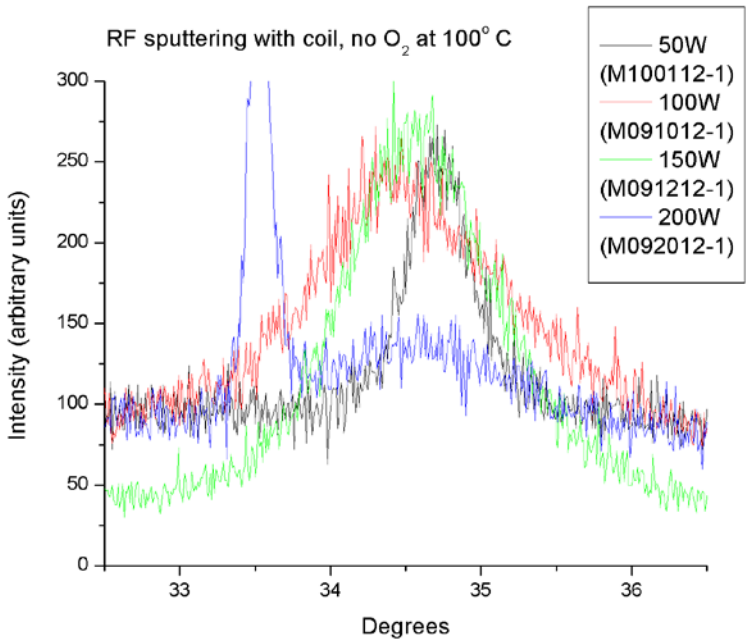

Figure 3.9 Samples produced at different RF power at 15 mtorr with an external magnetic field and no oxygen.

RF power (watts)	Thickness (nm)	Crystallite size
50	51 nm	0.22
100	51 nm	0.078
150	47.8 nm	0.069
200	48.0 nm	0.2

Table 3.5 Crystallite sizes computed from figure 3.13, and the thickness of each sample

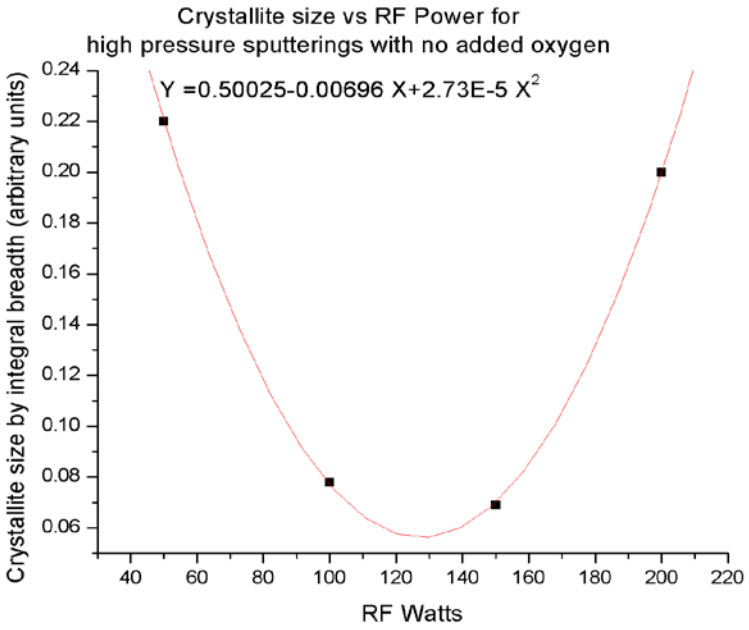

Figure 3.10 Crystallite sizes of samples from table 3.5 graphed against the wattage of the sputtering that produced the samples.

Four samples were sputtered in no oxygen, at 15mtorr, at 100˚ C with an external magnetic field at different wattages. These samples had different crystallite sizes, which were obtained from figure 3.12 and displayed in table 3.5. These crystallite sizes were graphed in 3.13 against their wattages. When fitted to a parabola, the minimum crystallite size is 128W.

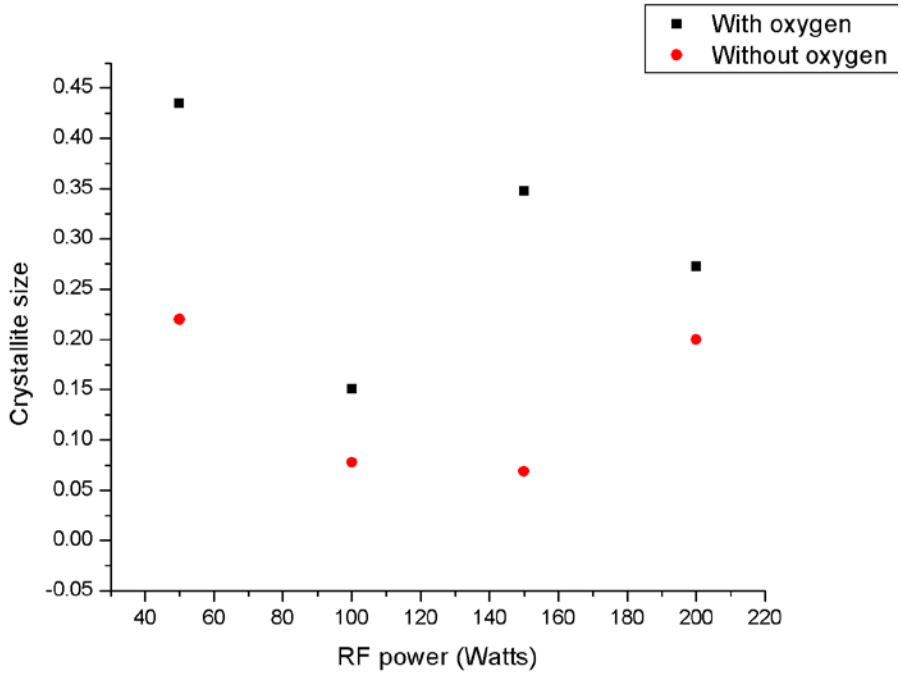

Figure 3.11 Samples graphed as in figure 3.14 (in red) with samples added that were produced in the same way in an oxygen environment.

Since figure 3.13 has so few data points, it is less easy to find it reliable. Figure 3.14 supports the trend found in figure 3.13, since adding the samples made in oxygen supports a parabolic trend (with the exception of the 150W sputtering). Each sputtering with oxygen gives larger crystallites than those produced without oxygen, as predicted in figures 3.7 and 3.8, which are represented here by the four data points at 150W and 200W. The thin films made using

oxygen do vary slightly when compared to those made not using oxygen. This could be due to variations in the amount of oxygen within the chamber.

RESISTIVITY MEASUREMENTS

Resistivity indicates the quality of the bulk material, rather than just the surface. The resistivity measurements were able to pick out a few samples as being well-made throughout, and a couple as not well made in spite of their crystal structure. Plotting resistivity vs. crystal structure reveals a relationship:

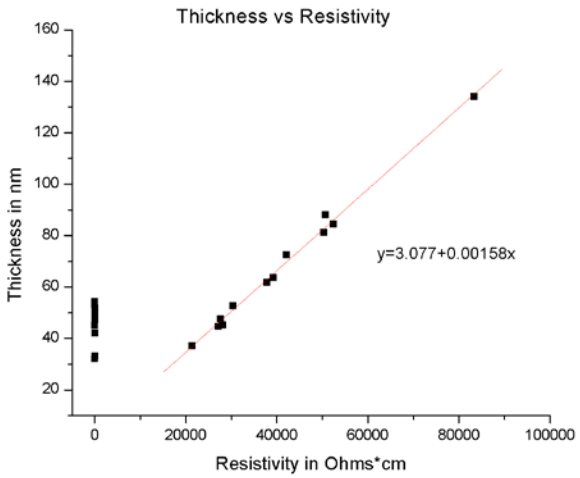

Figure 3.12 Thickness of samples vs their resistivity

The bulk resistivity increases as the thickness increases for many of the samples. This is most likely due to voids in the film, which might have more room to grow bigger in size and leave more voids in a thicker material. Some samples achieved quite a low resistance, which are clumped together as a line at the bottom left. Those samples form no trend of their own, but are independent of thickness, suggesting a consistent bulk structure without appreciable defects. Re-

graphing samples in terms of crystallite size, with those picked out of extremely low resistivity in red:

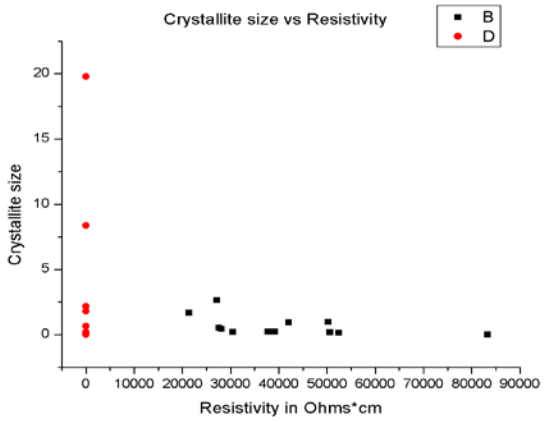

Figure 3.13 Crystallite size vs resistivity

The graph is decidedly non-random, as no samples have a high resistivity and large crystal size, which is to be expected, but the apparent randomness apart from that shows that many of the thin films are somewhat amorphous, even though many have a consistent bulk structure. The lowest resistivity measured for the samples was about 1000 times greater than that found for GZO previously in the literature. [18-19,29]

SCANNING ELECTRON MICROSCOPY (SEM)

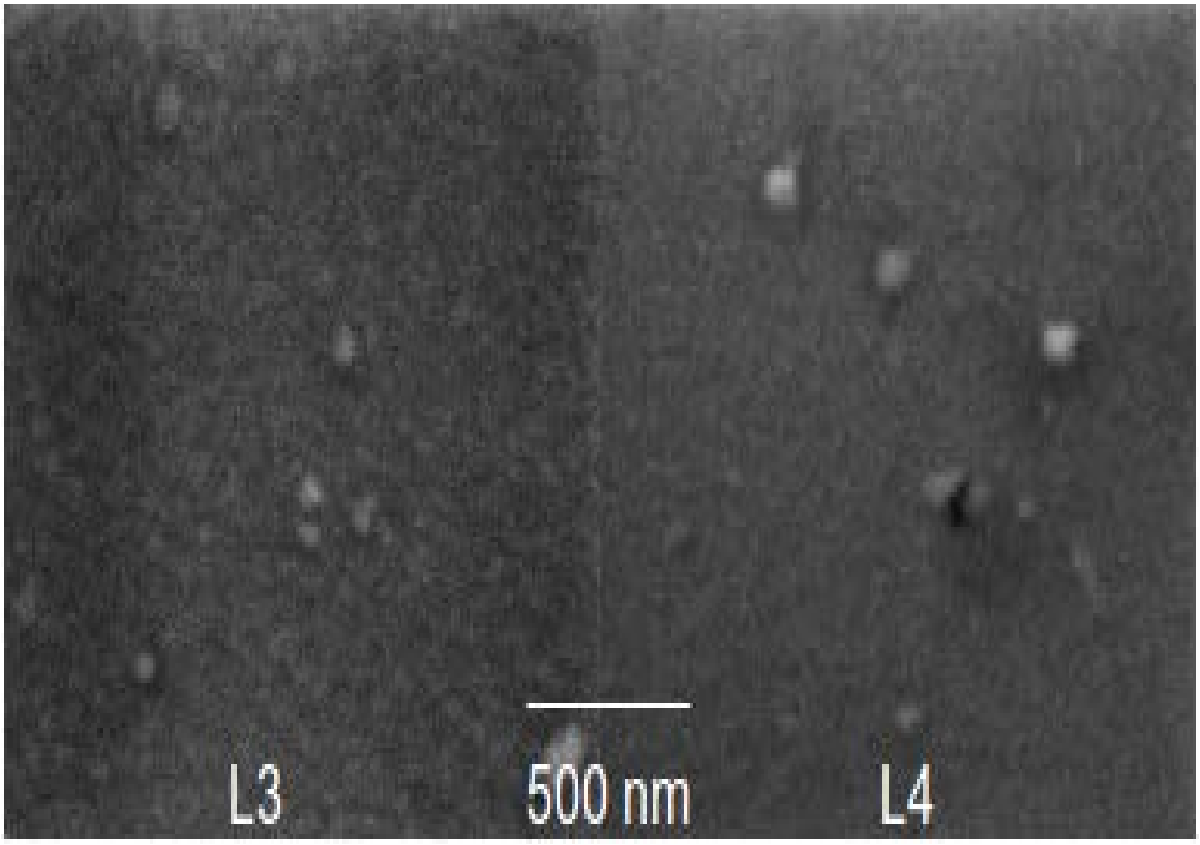

Figure 3.14 SEM of thin film samples L3 (crystallite size was shown to be around 0.52 by X-ray diffraction) and sample L4 (crystallite size 0.16)

Pictures of all hydrothermal samples and some thin films were taken using SEM. It was not possible to see crystallite size defects in the thin film samples by looking at SEM results alone, as may be seen in figure 3.14. These were two of the more clear SEM pictures and had higher resolution than most of the rest. It was found from X-ray diffraction that L3 had more

than three times the crystallite size that L4 did, which was one of the largest contrasts in the ZnO sputtered films. Some defects are visible, but many are likely due to post-manufacturing environmental factors. In figure 3.14, the inconsistency of each background might be a sign of how large particle size is at a smaller level, but the inconsistency is too small to measure, especially when larger obvious environmental defects are present.

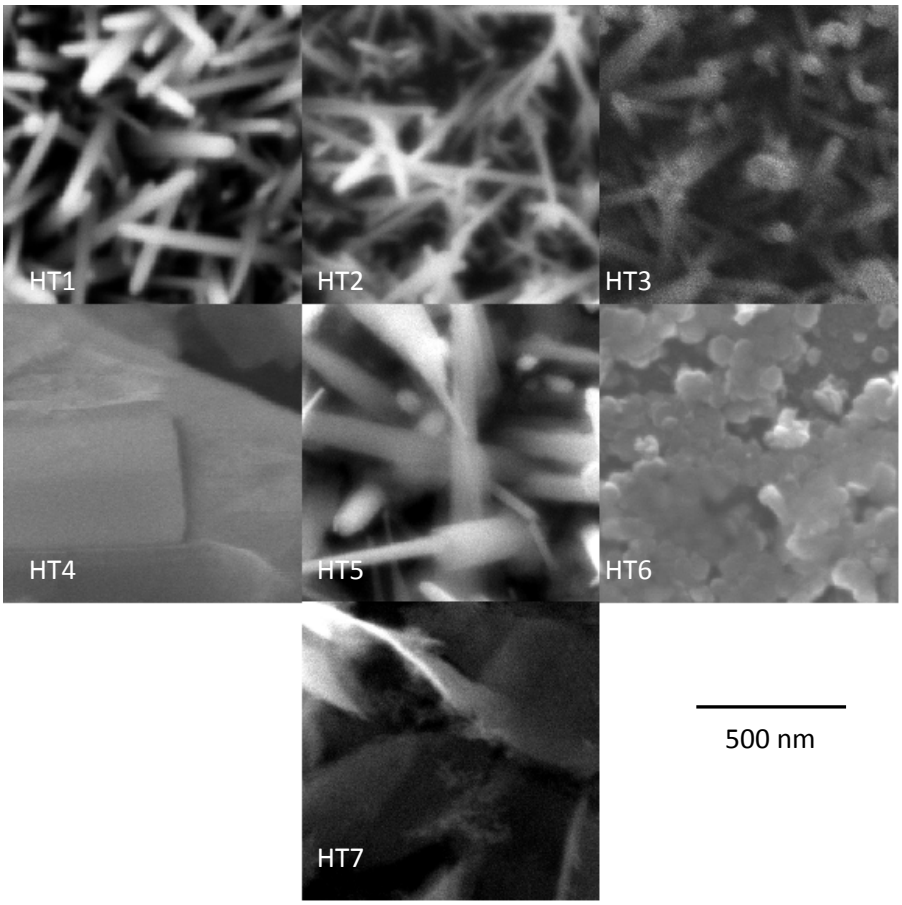

Figure 3.15 SEM of all hydrothermal samples. All samples, HT1-HT7, are at the same scale.

Pictures were taken of all hydrothermal samples using scanning electron microscopy. As seen in figure 3.15, samples HT1-HT5 all display nanowires. HT6 did not contain any consistent and well-defined nanostructure. HT7 contained nanopetals. Neither the density nor the presence of nanowires was measurably changed by gallium concentration. Since the last two samples

were made at a different time, it is most probable that an experimental difference led to the sample without nanostructures and the sample with nanopetals. More concentrated NaOH was used to stabilize these samples since they were so resistant to pH change. The pH was tested much sooner than the other samples, where there was an interval of 20-30 minutes. HT4 needed 15 drops of NaOH to stabilize its solution, and its nanowires were much larger than the others. It has previously been shown[42] that there are slight differences in morphology of nanowires with different concentrations of NaOH (though not too noticeable), however each of their starting solution began at different pH, rather than letting the solution destabilize and then stabilizing it with differing amounts of NaOH.

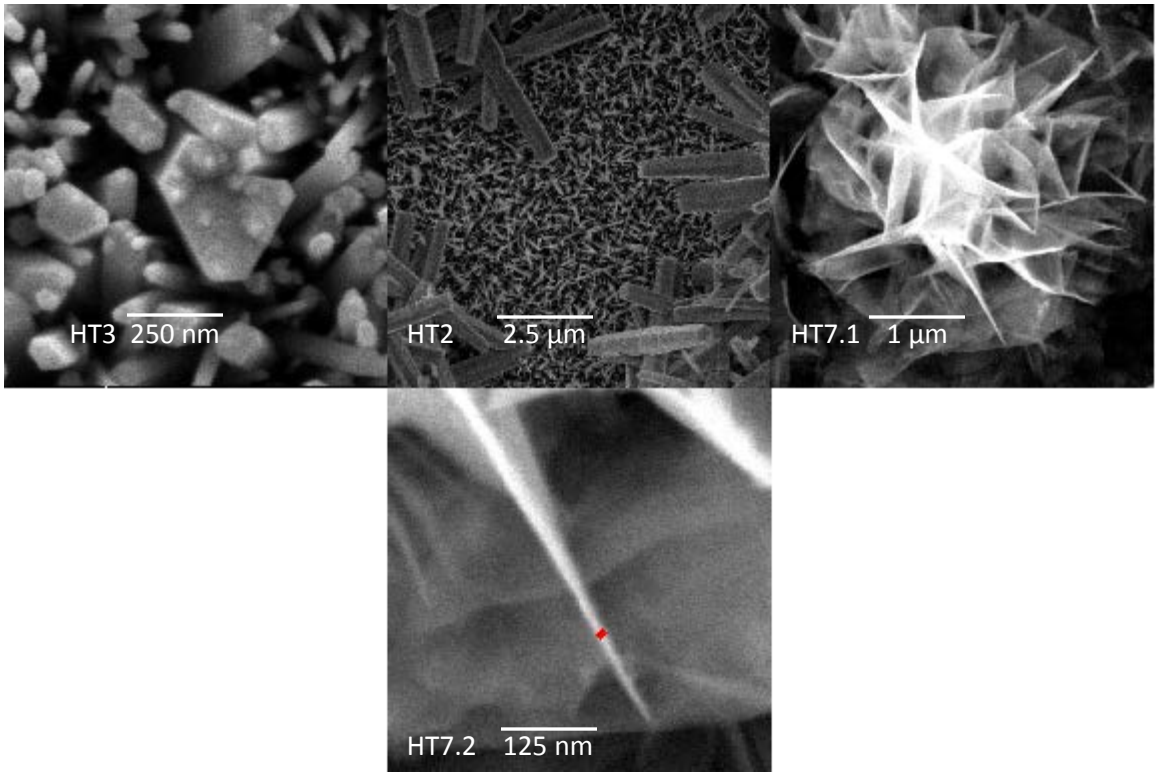

Figure 3.16 SEM pictures of select hydrothermal features. HT7.2 is a detail of HT 7.1 found just to the right of HT7.1's scale bar.

Figure 3.16 shows selected samples with a variety of features. The characteristic hexagonal structure can be most easily seen on HT3, whose nanowires were also vertically aligned. HT2 shows micro and nano structures grown on the same substrate, which was typical for most of the nanostructured samples. Finally, HT7 displayed nanopetals, which clumped together into a "flower" of sorts. Zooming in on one of the petals in HT7.2, a short red line was drawn to approximate the thickness of a petal whose cross-section was visible. From this, the maximum thickness of the petals can be estimated at around 15 nm. The length and width of these petals is on the order of a μm. From XPS, it was seen that this sample had roughly twice as many oxygen as zinc atoms, so there is a possibility that the different atomic ratio created a different structure. Currently, the most common way of producing zinc nanolayers such as these is to produce a nanowire and then uncurl it, but this suggests a different method for oxygen-rich GZO. If the petals themselves are the same sort of composition as the sample as a whole, there is a possibility that they, if easily manipulated, might be studied as something that could be attached to a substrate as a layer for a transistor, as they are about 1/3 as thick as the thin film layers, and cover very little area. It might be possible to use existing chemical methods for attaching GZO nanowires to substrates on these petals. Etching between transistors is presently about the same width that these petals are[17]. Some chemical methods exist[12-15] for sticking nanowires onto substrates, which might be used for sticking petals onto a substrate.

CONCLUSIONS

From the previous results, several conclusions may be reached. For sputtering GZO, smaller crystallite sizes result when:

- Sputtering is carried out at 15 mTorr rather than 5 mTorr
- Temperatures are higher
- A strong external magnetic field is turned on
- Oxygen is not present in the chamber during sputtering

The optimal power for sputtering 5% doped GZO is around 128 W. Despite optimizing these parameters, the bulk resistivity of the samples was far higher than those achieved by previous groups sputtering GZO. Unfortunately, differences in thin films could not be seen via SEM.

It was also shown that flat petal-like nanostructures could be grown by a chemical hydrothermal method. The petal structures were only about 15nm thick.

FURTHER STUDY

Further work could be done studying the “petals” that were produced after using the hydrothermal method with 5% doped gallium. Work could be done manipulating them and determining whether they could be chemically applied to a substrate. Further work could also be done in thin films, progressing towards manufacturing them by using substrates such as PET, and incorporating these transistor films into circuits for other sorts of testing.

REFERENCES

[1] DisplaySearch, *Monthly TFT LCD Shipment Database*

[2] Brody, TP et al, *IEEE Transactions on Electron Devices*, "A 6 x 6-in 20-lpi Electroluminescent Display" September 1975

[3] Arns, Robert G., *Engineering science and Education Journal*, "The other transistor: Early history of the metal-oxide-semiconductor field-effect transistor" Oct 1998

[4] *New York Times*, "The News of Radio" 1948

[5] Bell Telephone laboratories, Inc, *The Transistor*, Selected Reference Material on Characteristics and Applications, 1951

[6] Cobbold, Richard S C, *Theory and Applications of Field-Effect Transistors* Wiley-Interscience, 1970

[7] Neamen, Donald A., *Electronic Circuit Analysis and Design*, McGraw-Hill 2001

[8] Chang, Pai-Chung et al., High-performance ZnO nanowire field effect transistors *Applied Physics Letters* 89, 133113 (2006)

[9] Goldberger, Josh et al., ZnO Nanowire Transistors, *Journal of Phys Chem B Letters* 2005, 109, 9-14

[10] Ju, S et al., *Nano Lett*. 2005 Nov, 5(11):2281-6

[11] Fan, Zhihong and Lu, Jia G, "Electrical Properties of ZnO nanowire field effect transistors characterized with scanning probes" *Appl. Phys. Lett.* 86, 032111 (2005)

[12] Ahn, Jong-Hyun et al., "Heterogeneous Three-Dimensional Electronics by use of printed semiconductor nanomaterials" *Science* 15 Dec 2006 vol 314 no 5806 pp 1174-1757

[13] Yerushalmi, Roie et al., "Large Scale, highly ordered assembly of Nanowire parallel arrays by differential roll printing" *Appl. Phys. Lett.* 91, 203104 (2007)

[14] Chang, Yi-Kuei and Hong, Franklin Chau-Nan "The fabrication of ZnO nanowire field-effect transistors by roll-transfer printing" *Nanotechnology* 20 (2009) 195302

[15] Fan, Zhiyong et al., "Wafer-Scale Assembly of Highly Ordered Semiconductor Nanowire Arrays by Contact Printing" *Nano Letters* 2008 8 (1), 20-25

[16] *US Geological Survey*, Mineral Commodity Summaries, "Indium" January 2009

[17] Yamamoto, Naoki et al. Fine-line Patterning of Transparent Ga-doped ZnO Thin Films by Wet-etching *ECS Transactions*, 25 (27) 25-34 (2010)

[18] Schmidt, Nathan et al., "Effects of substrate temperature and near-substrate plasma density on the properties of dc magnetron sputtered aluminum doped zinc oxide"

[19] Gong, Li et al., *Solar Energy Materials & Solar Cells* 94 (2010) 937-941

[20] S Lee et al., *Semicond. Sci. Technol*. 26 (2011)115007

[21] Kim, Sookjoo et al., *J Mater Sci* (2007) 42:4845-4849

[22] Sheu, JK et al., *Journal of the Electrochemical Society*, 154 (6) H521-H524 (2007)

[23] W.T. Yen, et al., *Thin Solid Films* (2009), doi:10.1016/j.tsf.2009.10.149

[24] Xia Wu et al., 2012, *Advanced Materials Research*, 602-604, 1503

[25] Record of "Polyethylene terephthalate" in the *GESTIS Substance Database* from the IFA

[26] Shim, Jang Bo and Kim, Sung-O "Hydrothermal Synthesized Aluminum-Doped Zinc Oxide on Plastic Substrate"

[27] Hu, SY et al., *Applied Surface Science* 254 (2008)1578-1582

[28] Van de Pol, F. C. M, et al., *Thin Solid Films,* 204 (1991) 349-364

[29] Triboulet, R and Perriere, Jacques *Progress in Crystal Growth and Characterization of Materials* 47 (2003) 65-138.

[30] Assuncao, Vitor et al, *Thin Solid Films* 442 (003) 102-106

[31] Vayssieres, Lionel *Adv Mater*. 15 No 5, March 4 2003

[32] BE Deal and AS Grove "General relationship for the Thermal Oxidation of Silicon" *J. Appl Phys* vol 36 no 12 (1965) 3770

[33] Petrov et al, *J. Vac. Sci. Technol.* A 10, 3283 (1992)

[34] Lobachev, A. N. ed., *Hydrothermal Synthesis of Crystals* Consultants Bureau 1971

[35] L. Vayssieres *J. Phys. Chem. B* 2001, 105, 3350-3352

[36] M Wang et al., *J of Crystal Growth* 291 (2006) 334-339

[37] Sirota, Ben, *Synthesis and Characterization of ZnO2 and Bi2O3 nanowires grown by magnetron sputtering* 2009

[38] I Volintiru, Creatore and van Sanden, "In situ spectroscopic ellipsometry growth studies on the Al-Doped ZnO films deposited by remote plasma-enhanced metalorganic chemical vapor deposition" *J. Appl Phys* 103, 033704 (2008)

[39] Tompkins, Harland G and Irene, Eugene A, *Handbook of Ellipsometry* William Andrew 2005.

[40] Herzinger et al Thermal SiO2 *J. Appl Phys* 83 (1998) 3323

[41] Warren, B. E. *X-Ray Diffraction* Addison-Wesley Publishing Company 1969

[42] Aneesh, PM et al., "Synthesis of ZnO nanoparticles by hydrothermal method" *Proc. Of SPIE* Vol 66390J

APPENDICES

APPENDIX

Overall summary of sputterings. The left columns have the sputtering parameters, the columns on the right are characterizations of the sputtered samples. Samples are named "L" or "M" based on which machine produced them. "L" samples were made in Lucy, a sputter-down machine, while the other samples were made in Maggie, a sputter-up machine.

Sample name (L and M refer to sputtering machine used)	Gallium - doped= G, external coils on=C	Tem - pera-ture (˚C)	Time (minutes)	Power (watts) DC= direct current, RF= radio frequency	O2 pressure (mtorr)	Argon pressure (mtorr)	Bias (volts)		Thick -ness (nm)	Crystal size by FWHM (nm)	Crystal size by Integral breadth (arbitrary units)	Bulk Resis-tivity
L1		21	19	43 DC	1.1	5.0	0		52.73	0.3476	0.22	30400
L2		100	19	43 DC	1.0	5.0	0		63.63	0.2483	0.23	39200
L3		200	19	43 DC	1.25	5.0	0		47.62	0.2045	0.53	27600
L4		25	19	43 DC	0.8	5.0	-50		84.41	0.2897	0.16	52400
L5		25	19	43 DC	1.2	5.0	-100		58.98			52200
L6		100	19	43 DC	1.2	5.0	-50		45.2	1.2414	0.43	28100
L7		100	19	43 DC	0.8	5.0	-100		44.69	1.0223	2.65	27100
L8		200	19	43 DC	0.8	5.0	-100		87.97	0.1931	0.19	50600
L9		200	19	43 DC	0.8	5.0	-50		61.69	0.2633	0.24	37800
Hydro-thermal seed layers		25	40	50 RF	0.25-0.62	4.78-5.56	0		37-48			
M1		25	48	50 RF	~0.1	3.66	0		37.14	0.2897	1.67	21400
M2		200	48	50 RF	0.24	5.05	0		72.47	0.2897	0.94	42000

M3		100	48	50 RF	0.27	4.99	0		81.28	0.9656	0.96	50200
M4	G	26	30	50 DC	0.39	5.53	0		50	1.0223	1.80	12.9
M5	G	25	20	50 DC	0	5.36	0		33	0.1086	0.66	16.5
M6	G	27	30	50 DC	0	5.48	0		47.5	0.1053	0.20	5.06
M7	G, C	25	6	50 DC	0	~5.4	0		7.5		8.06	
M8	G	200	30	50 DC	0.18	5.32	0		49.2	0.4138	0.013	12.8
M9	G, C	200	6	50 DC	0.22	5.21	0		134	0.3476	0.019	83300
M10	G, C	25	9	50 RF	0	5.40	0		42.2	0.0939	8.37	6.87
M11	G, C	25	8	50 RF	0	5.51	0		51.8	0.0790	0.15	0.747
M12	G, C	25	8	50 RF	0	15.75	0		54.3	0.1022	19.79	0.0755
M13	G, C	200	8	50 RF	0	5.35	0		39	0.1086	0.079	
M14	G, C	100	8	50 RF	0	~15	-30		48.4			0.777
M15	G, C	100	~8	50 RF	0	~15	0		53.3			0.111
M16	G	100	~8	50 RF	0	~15	-30		45			0.316
M17	G	100	~8	50 RF	0	~15	0		32			0.123
M18	G, C	100				~15	0			0.4966	0.31	
M19	G, C	100	9	100 RF	0	~15	0		51	0.1511	0.078	
M20	G, C	100	6	100 RF	0	15.3	0		14.6	0.1448	0.22	
M21	G, C	100	6.5	150 RF	0	15.2	0		47.8	0.3476	0.069	
M22	G, C	100	10	100 RF	0.18	14.84	0		31.4	0.2287	0.25	
M23	G, C	100	10.5	150 RF	0.3	14.79	0		82.9	0.1121	0.23	
M24	G, C	100	5min 10s	200 RF	0	15.14	0		48	0.0848	0.20	
M25	G, C	100	7	200 RF	0.4	14.6	0		59.1	0.1159	0.27	
M26	G, C	100	19	100 RF	0.13	14.87	0		43.3	0.2759	0.21	
M27	G, C	100	25	50 RF	0	14.96	0		51	0.4345	0.22	
M28	G, C	100	~9	150 RF	~0.3	~14.7	0		50.7	0.2448	0.10	
M29		100	55	50 RF	0.28	14.7	0		64.6	Not seen		

VITA

Graduate School
Southern Illinois University

Timothy R Jones

tim.24.jones@gmail.com

St John's College at Annapolis
Bachelor of Liberal Arts, Great Books Program, May 2008

Thesis Title:
Manufacturing Gallium Doped ZnO Thin Films Suitable for Use in Thin Film Transistors Using Unbalanced Magnetron Sputtering

Major Professor: Dr Samir Aouadi